# An Evaluation of Digital Image Correlation Criteria for Strain Mapping Applications

W. Tong

Department of Mechanical Engineering, Yale University, New Haven, CT 06520-8284, USA

**ABSTRACT:** The performance of four digital image correlation criteria widely used in strain mapping applications has been critically examined using three sets of digital images with various whole-field deformation characteristics. The deformed images in these image sets are digitally modified to simulate the less-than-ideal image acquisition conditions in an actual experiment, such as variable brightness, contrast, uneven local lighting and blurring. The relative robustness, computational cost and reliability of each criterion are assessed for precision strain mapping applications. Recommendations are given for selecting a proper image correlation criterion to efficiently extract reliable deformation data from a given set of digital images.

**KEY WORDS:** *digital image correlation, image processing, in-plane strain measurement*

## NOTATION

| | |
|---|---|
| $B$ | The entire region of a sample surface common in both reference and current images |
| $C$, $C_{CC}$, $C_{SSD}$ | The generic, cross-correlation, and sum-squared difference image correlation coefficients |
| $C_1$, $C_2$, $C_3$, $C_4$ | Four specific sum-squared difference (SSD) image correlation coefficients |
| $\mathbf{E}$ or $E_{11}$, $E_{22}$, $E_{12}$ | The 2-D Lagrangian strain tensor and its three components |
| $\mathbf{F}$ | The deformation gradient tensor |
| $G(\mathbf{X}, t_0)$ | The brightness or greyscale value of each pixel of the reference image |
| $g(\mathbf{x}, t)$ | The brightness or greyscale value of each pixel of the current image |
| $N$ | The total number of valid pixels in an image subset $S$ |
| $\mathbf{P}$ or $P_1, P_2,\ldots,P_6, P_7$ | A set of parameters that define a possible local deformation mapping function for an image subset $S$ (usually centred at $\mathbf{X}_0$) |
| $\mathbf{P^*}$ or $P_1^*, P_2^*,\ldots,P_6^*, P_7^*$ | The parameters that define the optimised local deformation mapping function of an image subset $S$ |
| $S$ and $s$ | An image subset of the reference and current images respectively |
| $t_0$ | The time when the reference image $G(\mathbf{X}, t_0)$ is taken |
| $t = t_0 + \Delta t$ | The time when the current image $g(\mathbf{x}, t)$ is taken after a time increment $\Delta t$ |
| $\mathbf{u} = [u_1, u_2]$ | The 2-D displacement vector (and its horizontal and vertical displacement components) |
| $\mathbf{u}_p(\mathbf{X}; \mathbf{P})$ | The local displacement field of an image subset given by a set of deformation mapping parameters $\mathbf{P}$ |
| $w(\tilde{G}, \tilde{g})$ | The pixel-level weight function defined in terms of both reference and current images |
| $\mathbf{X} = [X_1, X_2]$ | 2-D Cartesian coordinates of a material point on the reference image $G(\mathbf{X}, t_0)$ |
| $\mathbf{X}_0$ | The centre or anchoring point of an image subset $S$ |
| $\mathbf{x} = [x_1, x_2]$ | 2-D Cartesian coordinates of a material point on the current image $g(\mathbf{x}, t)$. |

## Introduction

Various correlation criteria have been used in the literature for strain mapping measurements based on digital images [1–17]. Assessment of each criterion is often made individually based on the digital images acquired from nearly ideal test conditions and free from major image degradation. In an actual experimental environment, digital images are sometimes acquired with significant exposure and/or lighting variations over the loading history. Overexposure or underexposure, unstable or non-uniform lighting, uneven contrast, and blurring due to sample surface deformation and motion are among the most commonly encountered situations. There is a need to formulate a robust image correlation criterion and related image processing strategy for these images so the resulting strain mapping errors can be minimised or even eliminated.

This paper presents a study on the robustness, computational cost, and reliability of commonly used image correlation criteria by comparing their strain mapping results of three sets of numerically modified digital images with various degrees of average brightness, contrast and sharpness. In the following, a brief summary of the image correlation criteria evaluated in this study is first given. The procedure for selecting and generating the test image sets used in the study is then described. The strain mapping results obtained from correlation analyses of the test image sets using the various correlation criteria are presented. Finally, these results are discussed in terms of the strain mapping errors and the relative performance versus cost of these image correlation criteria.

## Criteria for Digital Image Correlation-Based Strain Mapping

For strain mapping and pattern recognition applications based on digital image correlation, several criteria for matching image pairs have been reported in the literature [1–21]. They will be summarised in the following using the notations adapted by Tong and Li [11] and Li [12]. Consider an object with a flat surface $B$ that lies on $X_1$–$X_2$ plane in the *initial* or *undeformed* configuration defined by the two-dimensional Cartesian coordinates ($X_1$, $X_2$) at a certain starting time $t_0$. The object is assumed to undergo only planar rigid-body motion and deformation so the surface $B$ remains flat and stays on $X_1$–$X_2$ plane. Let a material point $\mathbf{X} = [X_1, X_2]$ on the flat surface of the object displace to the location $\mathbf{x} = [x_1, x_2]$ at the time $t = t_0 + \Delta t$. The deformation equations in the Lagrangian formulation are defined as:

$$\mathbf{x} = \mathbf{x}(\mathbf{X},\ t) = \mathbf{X} + \mathbf{u}(\mathbf{X},\ t), \quad t \geq t_0, \tag{1}$$

where $\mathbf{u} = [u_1, u_2]$ is the displacement vector in the $X_1$–$X_2$ plane. The deformation gradient tensor $\mathbf{F}$ of an infinitesimal material vector at $\mathbf{X}$ is given as:

$$\mathbf{F} = \frac{\partial \mathbf{x}}{\partial \mathbf{X}} = \mathbf{I} + \frac{\partial \mathbf{u}}{\partial \mathbf{X}}, \quad \mathbf{X} \in B \text{ and } t \geq t_0. \tag{2}$$

The deformation gradient tensor $\mathbf{F}$ is used extensively in formulations of elasticity and plasticity deformation theories of materials. For example, the Lagrangian strain tensor $\mathbf{E}$ is computed via $\mathbf{E} = (\mathbf{F}^T\mathbf{F} - \mathbf{I})/2$.

During an experiment, the object surface $B$ at the times $t_0$ and $t$ are recorded respectively as *reference* and *current* images. In principle, the one-to-one correspondence between the physical and image coordinates of the object has to be established via a camera/lens calibration procedure. For simplicity, it is assumed that such a correspondence is identity so the spatial coordinates of the object in terms of pixels of digital images will be used in the remainder of the paper. Let $G(\mathbf{X}, t_0)$ and $g(\mathbf{x}, t)$ represent the brightness distribution functions of these two images in the *initial* (reference) and *deformed* (current) configurations respectively. The principle of image correlation for deformation measurement is to find a local displacement mapping $\mathbf{u}$ that can match the two intensity distribution functions over a small but finite area $S$ in the initial configuration ($S$ is called a *subset* of $B$ here) or over the corresponding area $s$ in the current configuration. The displacement mapping $\mathbf{u}$ over $S$ is often parameterised by a vector $\mathbf{P}$:

$$\mathbf{u}(\mathbf{X},\ t) = \mathbf{u}_\mathrm{p}(\mathbf{X};\ \mathbf{P}), \quad \mathbf{P} = \mathbf{P}(\mathbf{X}_0,\ t) = [P_1,\ P_2,\ P_3, \ldots], \tag{3}$$

where $\mathrm{X}_0$ is a reference material point usually centred within the subset $S$. The quality of matching between the two images over the subset region for an assumed parameter set $\mathbf{P}$ can be measured by a correlation coefficient:

$$C(\mathbf{X},\ t;\ \mathbf{P}) = C\{G(\mathbf{X},\ t_0),\ g(\mathbf{X} + \mathbf{u}_\mathrm{p},\ t)\}, \quad \mathbf{X} \in S, \tag{4}$$

where both the specific correlation criterion and the assumed displacement vector field $\mathbf{u}_\mathrm{p}(\mathrm{X};\ \mathbf{P})$ are defined over the subset $S$. Both cross-correlation (CC) criteria and sum-squared difference (SSD) correlation criteria have been proposed in the numerical and image analysis literature [18–21]. Consequently, the problem of deformation mapping by image correlation at an arbitrary point $\mathrm{X}_0$ located within the subset $S$ can be stated as to find a set of local mapping parameters $\mathbf{P}^* = [P_1^*,\ P_2^*,\ P_3^*, \ldots]$ that maximises a CC coefficient or minimises an SSD correlation coefficient:

$$C(\mathbf{P}^*) = \max_{\mathbf{P} \in \mathbf{P_D}} \{C_{\mathrm{CC}}(\mathbf{P})\}$$

or

$$C(\mathbf{P}^*) = \min_{\mathbf{P} \in \mathbf{P_D}} \{C_{\mathrm{SSD}}(\mathbf{P})\}, \tag{5}$$



 

where $\mathbf{P}_D$ contains all rational parameter sets of an assumed 2-D in-plane mapping function [e.g. def(**F**) > 0 is usually required]. To limit the scope of this study, only a homogenous deformation or affine mapping function will be considered, i.e. $\mathbf{P} = [P_1, P_2, P_3, P_4, P_5, P_6]$, with $P_1$ and $P_2$ as the two displacement components and $P_2$–$P_6$ as the four displacement gradient components. As CC coefficients are actually related to the SSD correlation coefficients [18–24], only the latter ones will be evaluated in this study. A generic SSD correlation coefficient can be defined as:

$$C_{SSD} = \int_S w\left(\tilde{G},\ \tilde{g}\right)\left[\tilde{g}(\mathbf{x},\ t) - \tilde{G}(\mathbf{X},\ t_0)\right]^2 dS, \tag{6}$$

where $\tilde{G}(\mathbf{X},\ t_0)$ and $\tilde{g}(\mathbf{x},\ t)$ are certain normalised forms of brightness distribution functions of the image pair $G(\mathbf{X},\ t_0)$ and $g(\mathbf{x},\ t)$ respectively, and $w(\tilde{G},\ \tilde{g})$ is a pixel-level weight function. Four commonly used SSD criteria are summarised in the following [assuming $w(\tilde{G},\ \tilde{g}) = 1$ and the total number of pixels within the subset is $N$]:

$$C_1 = \sum_{i=1}^{N} \frac{(g_i - G_i)^2}{\bar{G}^2} = 1 + \frac{\bar{g}^2}{\bar{G}^2} - \frac{2\sum_{i=1}^{N} g_i G_i}{\bar{G}^2}, \tag{7a}$$

$$C_2 = \sum_{i=1}^{N} \frac{(g_i + P_7 - G_i)^2}{\bar{G}^2} = 1 + \frac{(\bar{g} + P_7)^2}{\bar{G}^2} - \frac{2\sum_{i=1}^{N} (g_i + P_7) G_i}{\bar{G}^2}, \tag{7b}$$

$$C_3 = \sum_{i=1}^{N} \left(\frac{g_i}{\bar{g}} - \frac{G_i}{\bar{G}}\right)^2 = 2\left(1 - \frac{\sum_{i=1}^{N} g_i G_i}{\bar{g}\bar{G}}\right), \tag{7c}$$

$$C_4 = \sum_{i=1}^{N} \left(\frac{g_i - g_0}{\Delta g} - \frac{G_i - G_0}{\Delta G}\right)^2 = 2\left[1 - \frac{\sum_{i=1}^{N} (g_i - g_0)(G_i - G_0)}{\Delta g \Delta G}\right], \tag{7d}$$

where $P_7$ is an extra parameter accounting for variation of the local average brightness of the subset between the two images [8], and

$$\bar{g} = \sqrt{\sum_{i=1}^{N} g_i^2},\ g_0 = \sum_{i=1}^{N} \frac{g_i}{N},\ \Delta g = \sqrt{\sum_{i=1}^{N} (g_i - g_0)^2}, \tag{8a}$$

$$\bar{G} = \sqrt{\sum_{i=1}^{N} G_i^2},\ G_0 = \sum_{i=1}^{N} \frac{G_i}{N},\ \Delta G = \sqrt{\sum_{i=1}^{N} (G_i - G_0)^2}. \tag{8b}$$

As shown above, the CC coefficients are indeed related to the SSD coefficients (with additional assumptions of $\bar{g} = \bar{G}$ and $\bar{g} + P_7 = \bar{G}$ for $C_1$ and $C_2$ respectively). In this study, the minimisation problem of the SSD correlation coefficients with respect to either 6 or 7 local mapping parameters **P** was solved by the nonlinear Newton–Raphson method for least-squares regression [18]. Bicubic spline interpolation of the current image was used to compute the first-order spatial derivatives of the image brightness and subsequently to obtain the Jacobian (gradient) and approximate Hessian matrices for each correlation coefficient [8, 12]. The convergence conditions in the Newton–Raphson iterative routine were set to ensure that variations in displacements $P_1$ and $P_2$ were equal to or less than $10^{-4}$ pixel and variations in displacement gradients $P_2$–$P_6$ were equal to or less than $0.5 \times 10^{-6}$ (i.e. 0.5 $\mu$strains). A subset of $41 \times 41$ pixels and grids with $10 \times 10$ pixels were used in all analyses reported in the following.

## The Test Image Sets

Three sets of test images ($640 \times 480$ pixels, 8-bit greyscale) were used to evaluate the performance of various SSD correlation criteria. To simulate the different lighting conditions, the original images are modified using a commercial digital image-processing program (Paint Shop Pro, Eden Prairie, MN, USA). The first set of test images consists of a still digital image of an aluminium plate (about 25 mm wide) as shown in Figure 1A and its eight variations due to changes in lightning conditions, including 20% increase in brightness, 30% decrease in contrast, equalised histogram, blurring (Gaussian filtering), etc. The still digital images are used to assess the level of possible minimum errors introduced by the variable lighting conditions for small-strain mapping applications. The image pairs in the second set of test images are selected from a uniaxial tensile test of a compact dog bone-shaped steel sheet sample (Figure 1B). The width of the tensile sample is about 4.6 mm. The image of the deformed steel sheet sample is modified digitally to account for seven different lighting conditions. The second set of test images is used to evaluate the effects of variable lighting conditions on the local strains in a moderately and nominally homogenously deformed field. Finally, a pair of digital images from a tensile test of a tapered titanium sheet sample [14] is used as the basis for the third set of test images. The original width of the sample is about 4 mm and the image resolution is 9.7 microns per pixel (Figure 1C). The image of the deformed

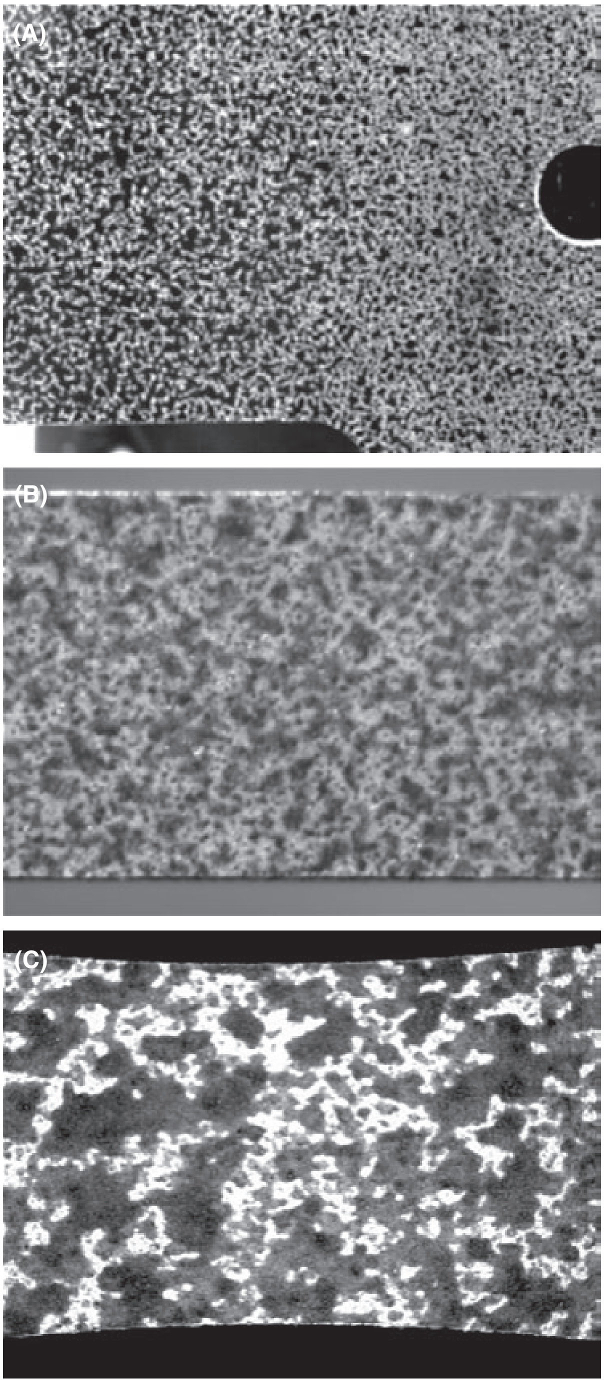


**Figure 1:** The reference images used in the current evaluation: (A) a stationary aluminum plate; (B) a steel sheet sample under uniaxial tension; (C) a tapered titanium sheet sample under uniaxial tension. The sample surfaces were decorated with spray black paint speckles to enhance the image contrast for image correlation processing

titanium sample is again modified digitally to account for seven different lighting conditions. The third set of images is used to evaluate the effects of variable lighting conditions on the overall strain distributions in a non-homogenous deformation field. The strain level is also much higher than that in the second image set. For a complete list of the digitally modified test images, see tables given in Appendix A.

## Evaluation Results

### The still image set

The eight image pairs (TST0 versus TST1-8) were evaluated according to the four SSD correlation criteria discussed above. Image correlation analysis results of the still image set are given in Tables 1–3 in terms of robustness, speed and reliability respectively. Table 1 shows the pass/fail results of digital image correlation calculations (here 'fail' means that the maximum iteration step of 80 was reached

**Table 1:** Summary of the robustness and speed (unit: minutes) for the first image set

| 'Lighting' conditions | $C_1$ | $C_2$ | $C_3$ | $C_4$ |
|---|---|---|---|---|
| +20% intensity (I) | 1.5 | 1.1 | 3.2 | 2.6 |
| −30% contrast (C) | 2.5 | 2.4 | 3.5 | 2.8 |
| −30% C and blurred | Fail* | Fail* | Fail* | 6.1 |
| Equalised histogram | 2.5 | 2.3 | 2.0 | 4.1 |
| Equalised and blurred | 1.8 | 1.7 | 2.0 | 5.2 |
| +20% I and −30% C | 3.3 | 2.4 | Fail* | 2.9 |
| +20% I, −30% C and blurred | Fail* | Fail* | Fail* | 5.3 |
| +20% I, −30% C and both | 1.9 | 1.8 | Fail* | 4.9 |

*Convergence conditions could not be reached at the end of 80 iteration steps.

**Table 2:** Global overall strains measured for the first image set (the unit for maximum global strain is micro-strains, i.e. $10^{-6}$)

| 'Lighting' conditions | $C_1$ | $C_2$ | $C_3$ | $C_4$ |
|---|---|---|---|---|
| +20% intensity (I) | 81 | <1 | 6.5 | <1 |
| −30% contrast (C) | 17 | 7.1 | 7.3 | 1.1 |
| −30% C and blurred | – | – | – | 3–6 |
| Equalised histogram | 90 | 15 | 5 | 1.9 |
| Equalised and blurred | 104 | 13 | 4.5 | 3.6 |
| +20% I and −30% C | 87 | 8.7 | – | <1 |
| +20% I, −30% C and blurred | – | – | – | 3–6 |
| +20% I, −30% C and both | 93 | 29 | – | 10–16 |

**Table 3:** Local strain mapping results for the first image set (the unit for the average and standard deviation in strains is micro-strains, i.e. $10^{-6}$)

| 'Lighting' conditions | $C_1$ | $C_2$ | $C_3$ | $C_4$ |
|---|---|---|---|---|
| +20% intensity (I) | 488 ± 2140 | <1 ± 3 | 22 ± 172 | <1 ± 3 |
| −30% contrast (C) | 70 ± 403 | 11 ± 144 | 22 ± 181 | <1 ± 8 |
| −30% C and blurred | – | – | – | 32 ± 147 |
| Equalised histogram | 375 ± 1485 | 49 ± 329 | 34 ± 161 | 3 ± 40 |
| Equalised and blurred | 582 ± 1801 | 85 ± 402 | 27 ± 166 | 23 ± 158 |
| +20% I and −30% C | 405 ± 1875 | 13 ± 142 | – | <1 ± 9 |
| +20% I, −30% C and blurred | – | – | – | 37 ± 149 |
| +20% I, −30% C and both | 667 ± 2386 | 157 ± 812 | – | 96 ± 743 |

without meeting the convergence conditions in the nonlinear Newton–Raphson solution procedure described above). The correlation criterion $C_4$ was most robust as no failure to converge was encountered while the criteria $C_1$ and $C_2$ were the second best (failed to process only two cases when both the image contrast was reduced and the image blurring was introduced). The correlation criterion $C_3$ was the least robust for this set of images (half of the eight image pairs failed to meet the convergence conditions). The total computational times that took to complete the successful image correlation calculations on a Pentium desktop computer are listed in Table 1 as well. The criteria $C_1$ and $C_2$ were among the fastest ones while the correlation criterion $C_4$ was the most computationally intensive (about half or less the speed of the fast ones on average).

The reliability and accuracy of the strain mapping results by digital image correlation were assessed in terms of both the global overall strain levels and the local strain variations (the average and the standard deviation of local strains). Tables 2 and 3 list the maximum values among the three in-plane strain components $E_{11}$, $E_{22}$ and $E_{12}$. Clearly, the criterion $C_4$ gave the most reliable and accurate results (i.e. closest to zero strains) for all cases compared. Uniform changes in intensity and/or contrast as well as equalisation in histogram induced little errors in both global and local strains using this criterion. Blurring of images induced about 30 $\mu$strains and 150 $\mu$strains in the average and standard deviation values of local strain levels. Little global strains (3–6 $\mu$ strains at most) were detected. However, significant errors in local strains existed for the images with non-uniform lighting changes (the last case in which three different regions in the image were modified separately (see Appendix A for details). As expected, the criterion $C_2$ was as accurate as the criterion $C_4$ in dealing with uniform shift in the image brightness. They were far less accurate in processing images undergoing a contrast shift or image blurring. Surprisingly, it also gave poor results for images with the histograms equalised. However, the criterion $C_3$ gave better results than the criterion $C_2$ for the histogram-equalised images (they are less robust though). For all the cases that could be processed successfully using the criterion $C_1$, the results were the worst in terms of both global and local strains.

## The homogenous deformation image set

The robustness and speed performance of the four correlation criteria are summarised in Table 4 for the second test image set. Both criteria $C_2$ and $C_4$ were equally robust in successfully processing all of eight pairs of images while the criterion $C_2$ was about three times faster than the criterion $C_4$. Using the original image pair, the three in-plane global strain components ($E_{11}$, $E_{22}$ and $E_{12}$) over the entire region of the strain maps have been computed as $0.04224 \pm 0.000628$, $-0.02235 \pm 0.000339$ and $0.000431 \pm 0.000331$ respectively. For all the cases that could be processed successfully, little difference was detected in the global overall strains. In many strain-mapping applications, details in the local strain distributions are of interest [5, 7, 12, 16]. The results obtained from using the original image pair based on the criterion $C_4$ may be used as the reference strain maps while all other results are treated as test strain maps. The differences between the test strain mapping results and the reference ones can then be computed. The standard deviations of the local point-to-point difference in three in-plane strain components can then be used as a measure of strain mapping errors (Table 5). The numbers in the brackets in Table 5 are the point-to-point CC coefficients [18] between the reference and test strain maps.

**Table 4:** Summary of the robustness and speed (unit: minutes) for the second image set

| 'Lighting' conditions | $C_1$ | $C_2$ | $C_3$ | $C_4$ |
|---|---|---|---|---|
| The original deformed image | 3.1 | 3.1 | 3.4 | 11.5 |
| +20% brightness | Fail* | 3.1 | 6.5 | 11.5 |
| −30% contrast and softened | 7.0 | 6.7 | 8.6 | 10.8 |
| Equalised histogram | Fail* | 9.3 | 7.8 | 14.4 |
| Equalised and blurred | Fail* | 7.7 | 6.4 | 14.1 |
| +20% I and −30% C (softened) | Fail* | 6.7 | Fail* | 10.8 |
| Gamma correction (0.65) | Fail* | 3.4 | 5.6 | 13.0 |
| Gamma correction (1.50) | Fail* | 3.4 | 6.3 | 12.0 |

*Convergence conditions could not be reached at the end of 80 iteration steps.

As expected, the criterion $C_4$ gave the best results for each case in terms of reliability. A simple shift in the image brightness or contrast induced little error using the criterion $C_4$. A softened image would have a local strain error of <100 $\mu$strains. Gamma corrections could cause the errors up to about 100–200 $\mu$strains or so. Equalised histogram and blurring would add the errors up to about 250–500 $\mu$strains and gave the smallest CC coefficient (much less than 0.9). The strain mapping results using the original pair of images and other three criteria show little errors (indicating the high quality of the original images; see case no.1 in Table 5). Again, the criterion $C_2$ was very effective in processing images with the simple shift in image brightness and somewhat effective with images subjected to gamma corrections. It was ineffective with images undergoing contrast changes, softening/blurring, and histogram equalisation. The criterion $C_1$ was least reliable as the

| 'Lighting' conditions | $C_1$ | $C_2$ | $C_3$ | $C_4$ |
|---|---|---|---|---|
| Original deformed image | 23 (0.93) | 32 (1.00) | 13 (1.00) | Reference maps |
| | 19 (0.88) | 35 (0.99) | 35 (0.99) | |
| | 10 (0.95) | 11 (1.00) | 7 (1.00) | |
| +20% brightness | – | 32 (1.00) | 1054 (0.67) | <1 (1.000) |
| | | 35 (0.99) | 1187 (0.54) | <1 (1.000) |
| | | 11 (1.00) | 368 (0.59) | <1 (1.000) |
| −30% contrast and softened | 1628 (0.57) | 989 (0.64) | 1184 (0.64) | 85 (0.99) |
| | 1687 (0.44) | 1191 (0.56) | 1357 (0.53) | 85 (0.97) |
| | 689 (0.42) | 344 (0.59) | 409 (0.55) | 42 (0.99) |
| Equalised histogram | – | 3846 (0.01) | 3616 (−0.13) | 266 (0.93) |
| | | 3934 (−0.28) | 3138 (−0.14) | 256 (0.73) |
| | | 1188 (0.36) | 1492 (0.16) | 140 (0.90) |
| Equalised and blurred | – | 4833 (0.02) | 4165 (−0.13) | 513 (0.80) |
| | | 4663 (−0.32) | 3752 (−0.16) | 429 (0.50) |
| | | 1448 (0.34) | 1745 (0.16) | 236 (0.81) |
| +20% I and −30% C (then softened) | – | 982 (0.65) | – | 91 (0.99) |
| | | 1186 (0.56) | | 85 (0.97) |
| | | 339 (0.60) | | 47 (0.99) |
| Gamma correction (0.65) | – | 251 (0.92) | 1628 (0.03) | 214 (0.94) |
| | | 244 (0.88) | 1633 (−0.05) | 149 (0.94) |
| | | 143 (0.91) | 648 (0.49) | 116 (0.94) |
| Gamma correction (1.50) | – | 378 (0.90) | 1209 (0.65) | 139 (0.98) |
| | | 333 (0.80) | 1256 (0.52) | 102 (0.95) |
| | | 129 (0.92) | 429 (0.54) | 75 (0.97) |

**Table 5:** Standard deviations of local strain differences d$E_{11}$, d$E_{22}$, d$E_{12}$ between test and reference strain maps for the second image set (the unit for local strain differences is micro-strains, i.e. $10^{-6}$ and the number in a bracket is the cross-correlation coefficients between the strain maps)

CC coefficients between the test and reference strain maps for cases other than no.1 were all far less than 0.9.

## The non-homogenous deformation image set

The original image pair in this image set was selected from the load steps nos. 22 and 38 of a consecutive image set that was analysed in an experimental study on diffuse necking in sheet metals [14]. As shown in Figure 2, axial strain distributions along the centre-line of the tapered tensile sheet sample have been found to be highly non-homogenous with increasing load steps. The robustness and speed performance of the four correlation criteria are summarised in Table 6 for the third test image set. The three in-plane global true strain components ($E_{11}$, $E_{22}$ and $E_{12}$) over the entire region of the strain maps have been computed using the original image pair and the criterion $C_4$ to be 0.2438 ± 0.06049, −0.1197 ± 0.03212 and 0.001950 ± 0.007358 respectively. Large standard deviations in strains are related to the highly non-homogenous deformation field itself (Figure 3). The correlation criterion $C_4$ was the most robust in successfully processing all eight pairs of images while the criterion $C_2$ was the second best (failed to process

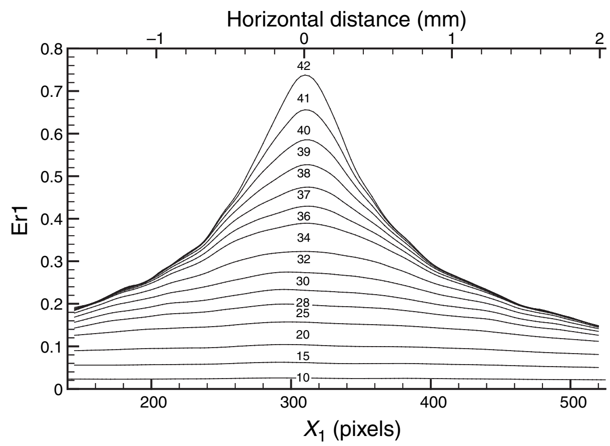


**Figure 2:** Axial strain distribution profiles at selected load steps for the tapered titanium sheet sample under uniaxial tension [14]. The numbers overlaid the curves are load steps when a digital image was taken during the test. The image pairs used here (TIP0 and TIP1) correspond to the one at load steps nos. 22 and 38 respectively

**Table 6:** Summary of the robustness and speed (unit: minutes) for the third image set

| 'Lighting' conditions | $C_1$ | $C_2$ | $C_3$ | $C_4$ |
|---|---|---|---|---|
| The original deformed image | 10.1 | 10.2 | 11.2 | 27.5 |
| +20% brightness | Fail* | 9.8 | 9.8 | 32.6 |
| +20% brightness and blurred | 12.9 | 12.2 | Fail* | 22.3 |
| Equalised histogram | Fail* | 10.9 | 16.1 | 35.7 |
| Equalised and blurred | Fail* | Fail* | Fail* | 29.9 |
| −30% contrast | 9.2 | 9.3 | 9.5 | 27.7 |
| −30% contrast and blurred | Fail* | Fail* | Fail* | 20.7 |
| +20% I and −30% C | 10.9 | 10.6 | Fail* | 32.6 |

*Convergence conditions could not be reached at the end of 80 iteration steps.

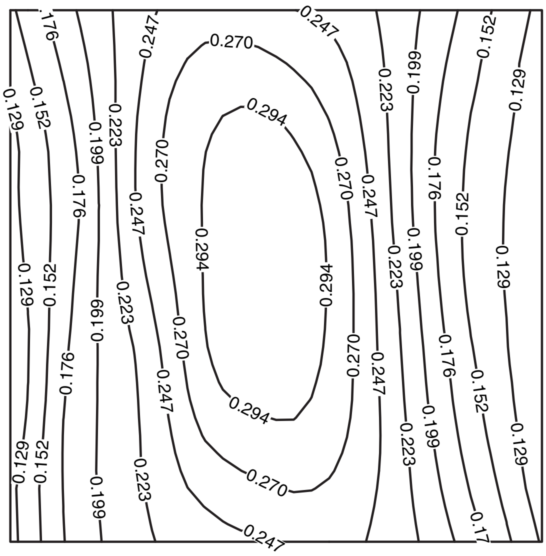


**Figure 3:** The axial true strain distribution of the tapered titanium sample between the original image pair of TIP0 and TIP1 (criterion $C_4$)

only two of the total eight cases). The criterion $C_1$ was the worst as it could only process four cases of them. Again, the criterion $C_2$ was about three times faster than the criterion $C_4$. For all the cases that could be processed successfully, little difference in the global strains were detected as well.

Similarly, the results obtained from the criterion $C_4$ and the original image pair may be used as the reference strain maps while all other results are regarded as test strain maps. The standard deviations of the local point-to-point difference between the test strain mapping results and the reference ones are shown in Table 7 for all three in-plane strain components. The numbers in the brackets in Table 7 are the CC coefficients between the reference and test strain maps. Another way of assessing the reliability of the strain mapping results is to use the normalised errors in local strains. The normalised local strain errors are computed by dividing the local strain difference (between the reference and the test maps) by the local strains of the reference maps. As an example shown in Figure 4 for the case no. 5 using the criterion $C_4$, the normalised error in the transverse strain component is at most a few per cent and is about only 0.1% at the centre of the tapered tensile sample. The criterion $C_2$ gave the local strain mapping reliability similar to that of the criterion $C_4$, except the case no. 6. The criterion $C_1$ had the worst reliability for this set of test images, especially for cases nos. 3 and 8.

## Discussions

Maintaining steady and uniform lighting and exposure conditions during image acquisition in a mechanical test is critical in achieving the best strain

**Table 7:** Standard deviations of local strain differences $dE_{11}$, $dE_{22}$, $dE_{12}$ between test and reference strain maps for the third image set (the unit for local strain differences is micro-strains, i.e. $10^{-6}$ and the number in a bracket is the cross-correlation coefficients between the strain maps)

| 'Lighting' conditions | $C_1$ | $C_2$ | $C_3$ | $C_4$ |
|---|---|---|---|---|
| The original deformed image | 972 (1.00) | 272 (1.00) | 500 (1.00) | Reference maps |
| | 539 (1.00) | 139 (1.00) | 285 (1.00) | |
| | 403 (1.00) | 70 (1.00) | 232 (1.00) | |
| +20% brightness | – | 2109 (1.00) | 3882 (1.00) | 2280 (1.00) |
| | | 1062 (1.00) | 1852 (1.00) | 1158 (1.00) |
| | | 790 (0.99) | 1575 (0.98) | 751 (1.00) |
| +20% brightness and blurred | 16880 (0.96) | 2310 (1.00) | – | 2530 (1.00) |
| | 8940 (0.96) | 1392 (1.00) | | 1481 (1.00) |
| | 6249 (0.80) | 959 (0.99) | | 867 (0.99) |
| Equalised histogram | – | 3795 (1.00) | 6192 (1.00) | 3684 (1.00) |
| | | 1906 (1.00) | 3087 (1.00) | 1821 (1.00) |
| | | 1309 (0.98) | 2382 (0.95) | 1077 (0.99) |
| Equalised and blurred | – | – | – | 4396 (1.00) |
| | | | | 2322 (1.00) |
| | | | | 1321 (0.98) |
| −30% contrast | 1523 (1.00) | 1517 (1.00) | 1312 (1.00) | 12 (1.00) |
| | 986 (1.00) | 838 (1.00) | 771 (1.00) | 8 (1.00) |
| | 599 (1.00) | 440 (1.00) | 647 (1.00) | 8 (1.00) |
| −30% contrast and blurred | – | – | – | 314 (1.00) |
| | | | | 557 (1.00) |
| | | | | 215 (1.00) |
| +20% I and −30% C | 10664 (0.98) | 1993 (1.00) | – | 2231 (1.00) |
| | 5220 (0.99) | 1192 (1.00) | | 1135 (1.00) |
| | 3930 (0.90) | 985 (0.99) | | 737 (1.00) |

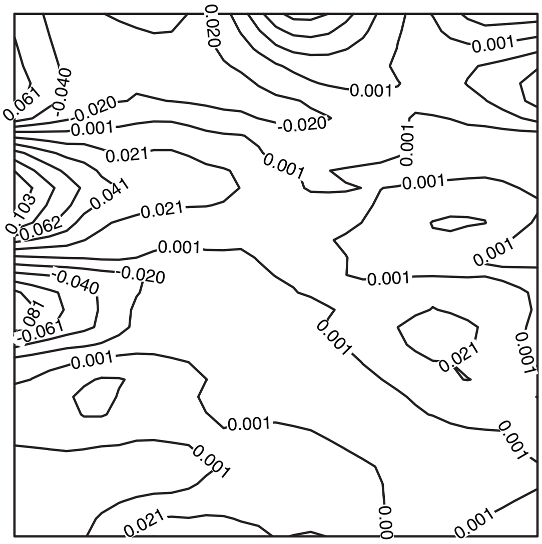


**Figure 4:** The normalised errors in transverse true strain distribution of the tapered titanium sample (case no. 5 listed in Table A3, criterion $C_4$)

mapping results by digital image correlation. When such conditions cannot be fully realised in an actual experiment due to either the limitation of the imaging hardware (especially the scanning electron and atomic force microscopes) or the surface degradation of deforming objects, the effect of variable lightings and exposures on the performance of digital image correlation-based strain mapping should be assessed and the most robust and reliable image processing strategy may be developed to minimise the measurement errors.

In all the successfully processed cases for the three sets of test images investigated here, the global average strain levels differ at most by 50–100 $\mu$strains. If such a level of errors is acceptable for a given application, then the variable lightning and exposure conditions simulated in this study is of little concern. The selection of the correlation criteria can be based on either the robustness (the criterion $C_4$) or the computational cost (the criterion $C_2$). However, when one is concerned with relatively small deformations of the order of a few hundreds micro-strains (≈0.01–0.1%) in either the overall average levels (the first test image set) or detailed local strain variations (the second test image set), the most robust and reliable correlation criterion $C_4$ should always be used. Unless the image pair to be processed is of highest quality, the strain mapping results obtained by other correlation criteria are always less reliable. Measurements of deformation fields with large overall strains and high strain gradients tend to be far less sensitive to the kinds of degradation of images considered here, although only the criterion $C_4$ is successful in processing all cases. The local measurements of the strain component $E_{12}$ (about 2700 $\mu$strains) in the third test image set become nevertheless unreliable.

Surprisingly, both criteria $C_1$ and $C_3$ have been used widely in a significant number of strain mapping applications [1–4, 6, 13, 16, 17]. While they may be adequate for pattern matching [20, 21] in general and whole-field strain mapping using images of very high quality, the results in this study have shown that both criteria are far less robust and reliable than either criterion $C_2$ or $C_4$. The correlation criterion $C_2$ was originally introduced in the context of processing 3-D surface profiling data acquired by scanning probe microscopy [8] and it has been used for many in-plane strain mapping applications [5, 7, 9, 11, 12, 14, 15]. The extra parameter $P_7$ effectively acts as a correction term on the average brightness of the image pair. While it is not as robust and reliable as the correlation $C_4$, its reduced computational cost makes it attractive for many practical applications. This study shows that the normalised correlation criterion $C_4$ is most robust and reliable for processing images with variable lightning or exposure problems considered here. Its only drawback is the threefold increase in the computational cost when compared with the criterion $C_2$.

## Conclusions

Based on the numerical evaluations of three sets of test images presented here, the performance of the four correlation criteria considered in this study can be summarised as following:

- Robustness ranking: $C_4$, $C_2$, $C_3$ and $C_1$;
- Reliability ranking: $C_4$, $C_2$, $C_3$ and $C_1$;
- Speed ranking: $C_1$, $C_2$, $C_3$ and $C_4$.

To achieve the most reliable results in strain mapping applications, the most robust correlation criterion $C_4$ should always be used. If only the average deformation levels of a deformed image are required or when images of good stability and minimal degradation can be assured, the fast correlation criterion $C_2$ may be used to reduce the computational cost. Other two correlation criteria evaluated here are not recommended at all for whole-field strain mapping measurements except for very high quality images.

### REFERENCES

1. Sutton, M. A., McNeill, S. R., Jang, J. and Babai, M. (1988) Effect of subpixel image restoration on digital correlation error estimates. *Opt. Eng.* **27**, 870–877.
2. Bruck, H. A., McNeill, S. R., Sutton, M. A. and Peters, W. H. (1989) Digital image correlation using Newton-Raphson method of partial differential corrections. *Exp. Mech.* **29**, 261–267.

3. James, M. R., Morris, W. L. and Cox, B. N. (1990) A high accuracy automated strain-field mapper. *Exp. Mech.* **30**, 60–67.

4. Franke, E. A., Wenzel, D. J. and Davison, D. L. (1991) Measurement of microdisplacements by machine vision photogrammetry. *Rev. Sci. Instrum.* **62**, 1270–1279.

5. Tong, W. (1997) Detection of plastic deformation patterns in a binary aluminum alloy. *Exp. Mech.* **37**, 452–459.

6. Choi, S. and Shah, S. P. (1997) Measurement of deformation on concrete subjected to compression using image correlation. *Exp. Mech.* **37**, 307–313.

7. Tong, W. (1998) Strain characterization of propagative deformation bands. *J. Mech. Phys. Solids* **46**, 2087–2102.

8. Vendroux, G. and Knauss, W. G. (1998) Submicron deformation field measurements, Part 2. Improved digital image correlation. *Exp. Mech.* **38**, 86–91.

9. Smith, B. W., Li, X. and Tong, W. (1998) Error assessment for strain mapping by digital image correlation. *Exp. Tech.* **22**, 19–21.

10. Zhang, D., Zhang, X. and Cheng, G. (1999) Compression strain measurement by digital speckle correlation. *Exp. Mech.* **30**, 62–65.

11. Tong, W. and Li, X. (1999) Evaluation of two plastic strain mapping methods. *Proc. SEM Annual Conference on Theoretical, Experimental and Computational Mechanics*, Cincinnati, Ohio, 23–26.

12. Li, X. (2000) Spatial characterization of unstable plastic flows in two aluminum alloys. PhD Thesis, Department of Mechanical Engineering, Yale University, New Haven, CT.

13. Schreier, H. W., Braasch, J. R. and Sutton, M. A. (2000) Systematic errors in digital image correlation caused by intensity interpolation. *Opt. Eng.* **39**, 2915–2921.

14. Tong, W. and Zhang, N. (2001) An experimental investigation of necking in thin sheets. *Proc. ASME Manufacturing Engineering Division MED*, New York, Vol. 12.

15. Raiser, G. F., Emery, R. D. and Tong, W. (2002) Digital image correlation – using deformation measurements to accelerate microprocessor product development. *Proc. SPIE – The International Society for Optical Engineering*, Vol. 4217, 485–490.

16. Wang, H. and Kang, Y. (2002) Improved digital speckle correlation method and its application in fracture analysis. *Opt. Eng.* **41**, 2793–2798.

17. Yoneyama, S. and Morimoto, Y. (2003) Accurate displacement measurement by correlation of colored random patterns. *JSME Int.* **A46**, 178–184.

18. Press, W. H., Flannery, B. P., Teukolsky, S. A. and Vetterling, W. T. (1986) *Numerical Recipes: the Art of Scientific Computing*. Cambridge University Press, Cambridge, UK: 484–485, 509–528.

19. Gonzalez, R. and Wintz, P. (1987) *Digital Image Processing*, 2nd edn. Addison Wesley, New York: 90–92, 100–109, 425–427.

20. Jain, R., Kasturi, R. and Schunck, B. G. (1995) *Machine Vision*. McGraw-Hill, New York: 482–483.

21. Ritter, G. X. and Wilson, J. N. (1996) *Handbook of Computer Vision Algorithms in Image Algebra*. CRC Press, Boca Raton, FL: 225–229.

22. Tong, W. and Zhang, N. (2004) On the crack initiation and growth in a strongly dynamic strain aging aluminum alloy sheet. *J. Mater. Sci. Technol.* **20** (Suppl. 1), 23–26.

23. Tong, W. (2004) An adaptive backward image correlation technique for deformation mapping of a growing crack in thin sheets. *Exp. Tech.* **28**, 63–67.

24. Tong, W. (2004) Plastic strain mapping of bent sheets by image correlation. *Exp. Mech.* **44**, 502–511.

## APPENDIX A: SUMMARY OF TEST IMAGE SETS

**Table A1:** The still image set

| Image file | Comments |
|---|---|
| TST0.RAW | The reference image (of an aluminium plate) |
| TST1.RAW | Brightness increased 20% from TST0 |
| TST2.RAW | Contrast reduced 30% from TST0 |
| TST3.RAW | Blurred TST2 |
| TST4.RAW | Histogram-equalised TST0 |
| TST5.RAW | Blurred TST4 |
| TST6.RAW | Brightness: +20% and contrast: −30% (TST0) |
| TST7.RAW | Blurred TST6 |
| TST8.RAW | Strip 1: brightness: +20% and contrast: −30%<br>Strip 2: only brightness increased 20%<br>Strip 3: only contrast reduced 30% (TST0) |

All digital image modifications mentioned above (and below) are carried out using the functions in the program Paint Shop Pro.

**Table A2:** The homogenous deformation image set

| Image file | Comments |
|---|---|
| STL0.RAW | The reference image (of a steel sample) |
| STL1.RAW | The deformed image (of the steel sample) |
| STL2.RAW | Brightness increased 20% from STL1 |
| STL3.RAW | Contrast reduced 30% from STL1 (softened) |
| STL4.RAW | Histogram equalised (STL1) |
| STL5.RAW | Blurred STL1 |
| STL6.RAW | Brightness: +20% and contrast: −30% from the image STL1 and then softened once |
| STL7.RAW | 0.65 gamma correction on STL1 (darker) |
| STL8.RAW | 1.50 gamma correction on STL1 (brighter) |

**Table A3:** The non-homogenous deformation image set

| Image file | Comments |
|---|---|
| TIP0.RAW | The reference image (of a titanium sample) |
| TIP1.RAW | The deformed image (of the titanium sample) |
| TIP2.RAW | Brightness increased 20% from TIP1 |
| TIP3.RAW | Blurred TIP2 |
| TIP4.RAW | Histogram equalised (TIP1) |
| TIP5.RAW | Blurred TIP4 |
| TIP6.RAW | Contrast reduced 30% from TIP1 |
| TIP7.RAW | Blurred TIP6 |
| TIP8.RAW | Brightness: +20% and contrast: −30% from the image TIP1 |